Dynamic reaction pathways of anionic products on the exit-channel potential energy surface for the reaction of O − with C 2H 4

ARTICLE *in* JOURNAL OF MOLECULAR STRUCTURE THEOCHEM · OCTOBER 2010

Impact Factor: 1.37 · DOI: 10.1016/j.theochem.2010.07.023

Journal of Molecular Structure: THEOCHEM 958 (2010) 41–47

Contents lists available at ScienceDirect

Journal of Molecular Structure: THEOCHEM

journal homepage: www.elsevier.com/locate/theochem

Dynamic reaction pathways of anionic products on the exit-channel potential energy surface for the reaction of O^- with C_2H_4

Feng Yu, Lixia Wu, Lei Song, Xiaoguo Zhou *, Shilin Liu

Hefei National Laboratory for Physical Sciences at the Microscale, Department of Chemical Physics, University of Science and Technology of China, Hefei, Anhui 230026, China

ARTICLE INFO

Article history:
Received 9 April 2010
Received in revised form 30 June 2010
Accepted 17 July 2010
Available online 23 July 2010

Keywords:
Atomic oxygen radical anion (O^-)
Ethylene (CH_2=CH_2)
Born–Oppenheimer molecular dynamics (BOMD)
Reaction mechanism

ABSTRACT

The dynamic reaction pathways after passing the initial barrier for the reaction of atomic oxygen radical anion (O^-) with ethylene (CH_2=CH_2) have been investigated with Born–Oppenheimer molecular dynamics (BOMD) simulations. The BOMD simulations initiated at this $[O\cdots H\cdots CH{=}CH_2]^-$ barrier on the exit-channel potential energy surface (PES) reveal several different types of dynamic reaction pathways leading to various anionic products. In particular, as the energy added on the transition vector of the $[O\cdots H\cdots CH{=}CH_2]^-$ transition state increases remarkably, the OH^- and CH_2=CH become the dominant products instead of the CH_2=CHO^- and H. As a result, animated images are displayed and more extensive reaction mechanisms are illuminated for the title reaction from the perspective of the dynamic reaction pathways.

1. Introduction

The reactions between atomic oxygen radical anion (O^-) and neutral molecules play important roles in many fields, such as ionospheric chemistry, combustion chemistry, radiation chemistry, chemical ionization mass spectrometry (CIMS), and so on [1]. Lots of chemically active negative ions can be generated directly from the reactions of O^- with neutral molecules [1,2]. For instance, vinylidene anion (CH_2=C^-) can be prepared in the reaction of O^- with ethylene (CH_2=CH_2) [3,4] and halogen substituted carbanions can be produced from the reactions of O^- with halogen substituted methanes [5]. Therefore, it is necessary to deeply investigate these reactions for ionospheric chemistry, combustion chemistry, organic chemistry, and analytical chemistry. Moreover, studying these reactions will give clues to the synthesis of organic intermediate anions and exploring the mechanisms for the liquid phase chemical reactions.

As summarized by Lee and Grabowski [1,3], there are four reaction channels listed as follows for the reaction between O^- and CH_2=CH_2,

$$\begin{aligned} O^- + CH_2{=}CH_2 &\rightarrow e^- + c\text{-}C_2H_4O \quad \text{Associative electron detachment},\\ &\rightarrow CH_2{=}C^- + H_2O \quad H_2^+ \text{ abstraction},\\ &\rightarrow CH_2{=}CHO^- + H \quad \text{H-atom displacement},\\ &\rightarrow OH^- + CH_2{=}CH \quad \text{H-atom abstraction}. \end{aligned}$$

These four reaction channels have been defined as associative electron detachment channel, H_2^+ abstraction channel, H-atom displacement channel, and H-atom abstraction channel, respectively. Because the CH_2=C^- is an important and chemically active anion [3], the title reaction has been extensively investigated with various experimental techniques. Bohme and Young [6] studied this reaction by employing a flowing afterglow (FA) apparatus, and only the associative electron detachment channel was observed. Stockdale et al. [7] detected OH^- and $C_2H_2^-$ as anionic products for the title reaction using a pulsed source mass spectrometer. A branching ratio of OH^- (20%) and $C_2H_2^-$ (80%) was deduced from the rate constants measured by Futrell and Tiernan using the tandem mass spectrometer [8]. Parkes [9] investigated this reaction using a drift tube with mass filter, and found that the associative electron detachment channel and H_2^+ abstraction channel were dominant. Goode and Jennings [10] confirmed that the molecular structure of the $C_2H_2^-$ product was CH_2=C^- indeed through examining the anionic products of the reaction between O^- and CH_2=CD_2 with ion cyclotron resonance (ICR) mass spectrometer. Lindinger et al. [11] studied the relative kinetic energy dependence for the title reaction by utilizing a flow-drift tube apparatus. The relative kinetic energy between O^- and CH_2=CH_2 was controlled by electric field and helium buffer gas number density. As they observed, the major anionic product was $C_2H_2^-$ with a trace of $C_2H_3O^-$ at a low relative kinetic energy of 0.0511 ev (~1.2 kcal mol^{-1}), while the OH^- became dominant at a higher relative kinetic energy of 1.14 ev (~26.3 kcal mol^{-1}) with the $C_2H_3O^-$, C_2HO^-, and $C_2H_2^-$ followed as minor products. Dawson and Jennings [12] observed only

* Corresponding author. Tel.: +86 551 3600031; fax: +86 551 3602323.
E-mail address: xzhou@ustc.edu.cn (X. Zhou).

0166-1280/$ - see front matter © 2010 Elsevier B.V. All rights reserved.
doi:10.1016/j.theochem.2010.07.023

$CH_2{=}C^-$ as anionic product with the ICR mass spectrometer. Viggiano and Paulson [13] investigated the temperature dependence of the title reaction using a selected ion flow tube (SIFT) apparatus, and found that the associative electron detachment channel and H_2^+ abstraction channel were dominant. The corresponding rate coefficients dropped as the temperature increasing, and however the branching ratios did not present obvious dependence on temperature. Obviously, different studies present different results due to the different experimental conditions and anion detection techniques. Although reaction mechanisms have been proposed from the detected anionic products [1], the corresponding details of the reaction processes are still unknown. Therefore, static and also dynamic reaction pathways should be followed based on theoretical calculations.

Recently, we have theoretically investigated the title reaction at a high level of theory [14]. An extensive potential energy profile was mapped, and the branching ratios obtained from previous experiments [6–13] were also qualitatively explained based on the calculated barrier heights on the potential energy profile. However, only the static reaction pathways have been considered, and the dynamic reaction pathways involved in the real reaction processes cannot be obtained from the potential energy profile. Furthermore, a secondary reaction of O^- with vinyl radical ($CH_2{=}CH$) for the title reaction has also been studied to clarify the influence of the potential secondary reaction [15]. Zhao et al. [16] have theoretically investigated the potential energy profile and corresponding reaction mechanism for the reaction of O^- with propene ($CH_3{-}CH{=}CH_2$), in which the reaction processes are very similar to those of the reaction between O^- and $CH_2{=}CH_2$ [14].

The anionic products can be produced via the isomerization and subsequent dissociation of the intermediate complexes from a view of the static reaction pathways revealed by the potential energy profiles. However, according to the dynamic reaction pathways, these anionic products can be probably generated without undergoing the intermediate complexes [17–20]. Therefore, to obtain a comprehensive reaction mechanism, both the static and dynamic reaction pathways on the potential energy surface (PES) are necessary to be followed on the basis of quantum chemical calculations. At the initial stage of the reaction between O^- and $CH_2{=}CH_2$, O^- approaches $CH_2{=}CH_2$ quickly to form an ion-induced dipole complex, and then this intermediate complex overcomes the $[O\cdots H\cdots CH{=}CH_2]^-$ barrier to form another intermediate complex, which will decompose to various products subsequently [14]. In order to present the dynamic images for various production channels, the dynamic reaction pathways after passing the aforementioned barrier are explored with Born–Oppenheimer molecular dynamics (BOMD) simulations [21–23] in this work. In addition, we also investigate the dynamic effect on the transition vector excitation, and thus, more comprehensive reaction processes are obtained to explain the observed dependence of the branching ratios of the anionic products on the relative kinetic energy of reactants, which is another significant motivation for us to reinvestigate the title reaction.

2. Computational methods

All the present BOMD simulations were carried out with the Gaussian 03 program package [24]. The quadratically convergent self-consistent-field (QCSCF) method [25] was employed to overcome the SCF convergence problems encountered in this open-shell reactive system. As mentioned in our previous work [14], the B3LYP/6-31+G(d,p) level of theory [26,27] cannot give very accurate energies for the stationary points on the PES, however, it can characterize the PES for the title reaction. For example, this level of theory has been successfully utilized to map the potential energy profile [28] and investigate the dynamic reaction pathways [29] for the reaction between O^- and CH_3F. Therefore, we also chose this level of theory to perform the present BOMD simulations, especially with respect to the computational cost. It is worthy to note that the BOMD simulation cannot deal with the associative electron detachment process, and therefore, we only paid our attention to the dynamic reaction pathways leading to the anionic products in this work.

Briefly, the dynamic trajectories were integrated by utilizing the Hessian-based predictor–corrector algorithm with Hessian updating for 5 steps on the Born–Oppenheimer PES at the B3LYP/6-31+G(d,p) level of theory [30,31]. The step size for all the trajectories was set as 0.25 $amu^{1/2}$ bohr, and the trajectories would be stopped when the center of mass distance of the dissociating fragments was more than 15 bohr or the total steps exceeded the maximal points of 3500. In order to investigate the microscopic dynamics on the exit-channel PES, these trajectories were initiated at the $[O\cdots H\cdots CH{=}CH_2]^-$ barrier as mentioned above. Initial conditions were determined by the thermal sampling [32,33]. The vibrational and rotational sampling temperatures were both set to be 300 K, and the zero point energies (ZPEs) were also incorporated into the vibrational sampling. The transition vector was determined to point to the products, and the energies added on this imaginary vibrational mode were set to be 1.0, 5.0, 25.0, and 35.0 kcal mol^{-1}, respectively, to investigate the relative kinetic energy dependence of the dynamic reaction pathways.

With respect to the relative kinetic energy and ion-induced dipole interaction, the reaction of O^- with $CH_2{=}CH_2$ is very fast with an overall reaction rate of 9.0×10^{-10} $cm^3\ s^{-1}$ at 300 K [13]. As a result, along the process of O^- attacking a H atom of $CH_2{=}CH_2$, the relative kinetic energy and release of the potential energy (the energy of the $[O\cdots H\cdots CH{=}CH_2]^-$ barrier is below that of the reactants on the PES [14]) will mainly distribute into the transition vector of the $[O\cdots H\cdots CH{=}CH_2]^-$ barrier. Therefore, the energy added on the transition vector is directly related to the relative kinetic energy between O^- and $CH_2{=}CH_2$. Additionally, according to the previous experimental result [13], the production branching ratios of the reaction between O^- and $CH_2{=}CH_2$ present no obvious dependence on the temperature. Thus, we have not utilized the thermal sampling for the transition vector along with the vibrational and rotational degrees of freedom at different temperatures.

A total of 220 trajectories have been calculated for the current thermal sampling with transition vector excitation, and the trajectories with SCF convergence problems are discarded. The relative energies of these trajectories drift within a range from 10^{-3} kcal mol^{-1} to 1 kcal mol^{-1}, and the relative angular momentums float within a range between 10^{-9} ħ and 10^{-7} ħ. Although an accurate branching ratio for each reaction channel and energy distributions for the products cannot be evaluated from these 220 trajectories, the dynamic reaction pathways and corresponding reaction mechanisms can be obtained definitely based on our BOMD simulations. Actually, to elucidate the dynamic reaction pathways and corresponding reaction mechanisms are exactly the most important goal for this study.

Moreover, the BOMD simulations performed on different revisions of the Gaussian 03 program running on different computer platforms maybe show different single trajectory due to the numerical errors, but the conclusions and discussions based on a certain amount of trajectories will not be influenced essentially. Furthermore, as mentioned above, the total energies and total angular momentums of our calculated trajectories are conserved well, and the initial condition for each trajectory is determined randomly. We have calculated 55 trajectories for each sampling with different energy specified on the transition vector in the present work. According to the previous direct dynamics simulations [17,34], our calculations are enough to elucidate the dominant

channels for the reaction of O^- with $CH_2{=}CH_2$. Additionally, the Mulliken population analysis [35] is utilized to characterize the charge distributions for the intermediate complexes and anionic products.

3. Results and discussion

3.1. Brief summary of the static reaction pathways

A potential minimum denoted as IM1 ($O^-\cdots HCH{=}CH_2$) is found by the reverse intrinsic reaction coordinate (IRC) calculation for the $[O\cdots H\cdots CH{=}CH_2]^-$ barrier (denoted as TS1 in Fig. 1). The IM1 is a hydrogen bond complex formed by the collision between O^- and $CH_2{=}CH_2$. The forward IRC calculation points to another potential minimum denoted as IM2 ($CH_2{=}CH{-}OH^-$), and the corresponding static reaction pathway is the O^- insertion process indeed. The schematic diagram for the IRC profile is shown in Fig. 1, and obviously all the anionic products detected by previous experiments [6–13] can be derived from IM2. The C—O bond cleavage of IM2 leads to $OH^- + CH_2{=}CH$ as products, and the break of the O—H bond can produce the $CH_2{=}CHO^-$ and H. On the other hand, when the dissociating OH^- roams towards the $CH_2{=}CH$ moiety and abstracts a proton, the $CH_2{=}C^- + H_2O$ or $CH{\equiv}CH^- + H_2O$ will be produced at last. As indicated in previous calculations [14], TS1 is the rate-determining barrier for the formation of anionic products, therefore, this barrier is the most important stationary point on the reaction PES and its features will determine the reaction dynamics between O^- and $CH_2{=}CH_2$.

3.2. Dynamic reaction pathways revealed by the BOMD simulations

In order to obtain the dynamic reaction pathways after passing the TS1, a total of 220 trajectories have been calculated via the BOMD simulations. A brief summary of these trajectories has been listed in Table 1. When the energy added on the transition vector of the TS1 is 1.0 kcal mol^{-1}, the dominant products are confirmed to be $CH_2{=}CHO^-$ and H. With the energy added on the transition vector increased from 1.0 kcal mol^{-1} to 5.0 kcal mol^{-1}, the $CH_2{=}C^- + H_2O$ production channel becomes more important. The major production channels are $OH^- + CH_2{=}CH$ and $CH_2{=}C^- + H_2O$ when the energies added on the transition vector are both 25.0 and 35.0 kcal mol^{-1}. As noticed in Table 1, some trajectories stop at the stage of the $CH_2{=}C^-\cdots H_2O$ intermediate complex within limited maximal steps, which are expected to dissociate to $CH_2{=}C^- + H_2O$ finally with additional steps. Therefore, with respect to these trajectories, the branching ratio for the $CH_2{=}C^- + H_2O$ production channel will increase dramatically in the cases that the energies added on the transition vector are 1.0 and 5.0 kcal mol^{-1}.

Table 1
Trajectory summary for the title reaction after passing the $[O\cdots H\cdots CH{=}CH_2]^-$ barrier.

Reaction channels	Energies added on the transition vector of the $[O\cdots H\cdots CH{=}CH_2]^-$ barrier (kcal mol^{-1})			
	1.0	5.0	25.0	35.0
$CH_2{=}CHO^- + H$	26	20	2	7
$OH^- + CH_2{=}CH$	8	3	16	22
$CH_2{=}C^- + H_2O$	7	15	26	19
$CH{\equiv}CH^- + H_2O$	0	2	5	1
$O^- + CH_2{=}CH_2$	0	0	1[b]	2[b]
Other trajectories[a]	14	15	5	4
Total	55	55	55	55

[a] These trajectories do not meet the stopping criteria within 3500 steps. There are 13, 15, 3, and 2 trajectories which result in the dynamic $CH_2{=}C^-\cdots H_2O$ intermediate complex when the energies added on the transition vector of the $[O\cdots H\cdots CH{=}CH_2]^-$ barrier are 1.0, 5.0, 25.0, and 35.0 kcal·mol^{-1}, respectively.
[b] These three minor trajectories are obtained with the Gaussian 03, revision C.02, which may encounter the SCF convergence problem in revision D.01 and D.02. However, this issue will not influence our results seriously.

Although the accurate branching ratios cannot be evaluated from these 220 trajectories, we are able to deduce the major anionic products based on the current BOMD simulations, with assuming that the energy added on the transition vector is directly related to the relative kinetic energy between O^- and $CH_2{=}CH_2$. The dominant products are $CH_2{=}CHO^- + H$ and $CH_2{=}C^- + H_2O$ when the relative kinetic energy is low. However, when the relative kinetic energy is relatively high, the major products are $OH^- + CH_2{=}CH$ and $CH_2{=}C^- + H_2O$. These conclusions are

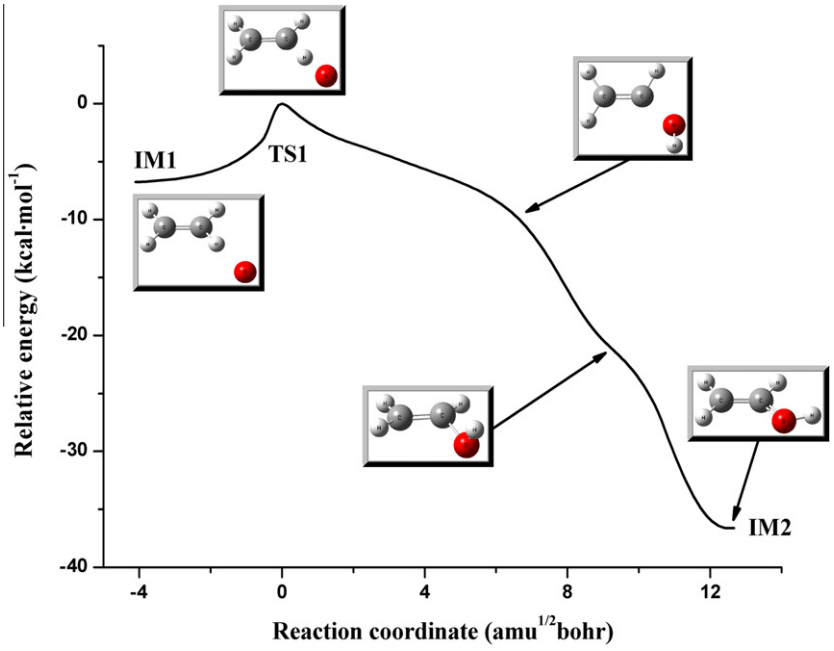

Fig. 1. Potential energy profile along the IRC for the $[O\cdots H\cdots CH{=}CH_2]^-$ barrier (TS1). The reverse IRC points to IM1 ($O^-\cdots HCH{=}CH_2$), and the forward leads to IM2 ($CH_2{=}CH{-}OH^-$). Five typical molecular geometries along the IRC profile are also shown.

consistent with previous experimental results [11]. The slight disagreement may arise from the secondary reactions in the reaction tube and the limited number of trajectories. Lee and Grabowski [1] have summarized the experimental results for the title reaction. According to their review, the associative electron detachment channel is the major production channel and the CH_2=C^- is the dominant anionic product. However, the associative electron detachment process is beyond the scope of the present trajectory calculations, because the BOMD simulations with the B3LYP method cannot model this type of process.

3.3. Reaction mechanisms uncovered by the BOMD simulations

The static intermediate complexes, such as the IM1 and IM2 mentioned in Section 3.1, are the stationary points without imaginary frequencies on the reaction PES. Unlike them, the dynamic intermediate complexes are those special stages on the dynamic trajectories, which are usually trapped in potential wells for a period of time with the molecular structures changing from time to time. Generally speaking, their molecular structures are a certain extent similar to the corresponding static intermediate complexes. In the following discussions, all the intermediate complexes referred are the dynamic intermediate complexes unless otherwise noted, since our most attentions are paid to dynamic reaction pathways in the present work.

For the dynamic reaction pathways leading to the products of CH_2=CHO^- and H, the distances between C1 atom and H2 atom along a typical trajectory are shown in Fig. 2. Along this trajectory, the reactive system firstly falls into a deep potential well of CH_2=CH—OH^- to form a dynamic intermediate complex. After being trapped for about 500 fs, the reactive system dissociates to CH_2=CHO^- + H as products at last. All other trajectories leading to CH_2=CHO^- and H are similar to this trajectory in our calculations. For some of them, the lifetimes of the CH_2=CH—OH^- dynamic intermediate complexes are very short, and the C—O bond formation and the O—H bond rupture are nearly simultaneous. Obviously, the geometry of the dynamic intermediate complex of CH_2=CH—OH^- looks like that of the IM2 in Fig. 1. Therefore, this type of dynamic reaction pathway involving the dynamic CH_2=CH—OH^- intermediate complex is consistent with the static reaction pathway in Fig. 1, which leads to the IM2 in the forward direction.

There are two major types of trajectories which lead to OH^- + CH_2=CH as products. The distances between C1 atom and O atom along two corresponding typical trajectories are shown in Fig. 3, respectively. Along the first one, the TS1 directly decomposes to OH^- and CH_2=CH without involving any intermediate complex. Interestingly, the energy added on the transition vector of the TS1 makes the reactive system deviate from the minimum energy path (MEP) which leads to the deep CH_2=CH—OH^- potential well, i.e. this type of trajectory bypasses the CH_2=CH—OH^- potential well as indicated in Fig. 3(a). This mechanism is important for the H-atom abstraction channel, because it provides insight into the direct H-atom abstraction process between O^- and organic molecule. As shown in Fig. 3(b), a dynamic intermediate complex of $OH^-\cdots$CH=CH_2 is formed at the first stage of the reaction process along the second type of trajectory, and then it dissociates to the final products of OH^- and CH_2=CH. Moreover, a few trajectories of this type also involve the CH_2=CH—OH^- intermediate complex before the formation of the $OH^-\cdots$CH=CH_2 intermediate complex.

Fig. 4 shows the distances between C1 atom and O atom along a typical trajectory of the dynamic reaction pathways leading to CH_2=C^- + H_2O. Along this trajectory, the TS1 firstly dissociates to OH^- fragment and CH_2=CH fragment, and then the dissociating OH^- fragment roams around and abstracts a proton of the CH_2=CH fragment. Therefore, a CH_2=$C^-\cdots H_2O$ intermediate complex is formed instead of the separation between the OH^- fragment and CH_2=CH fragment. Subsequently, the CH_2=$C^-\cdots H_2O$ intermediate complex decomposes to CH_2=C^- and H_2O at last. Furthermore, as noted in Table 1, the trajectories leading to the CH_2=$C^-\cdots H_2O$ intermediate complex also undergo a similar proton abstraction process, and these trajectories will dissociate to the final products of CH_2=C^- and H_2O with additional steps. On the other hand, if the dissociating OH^- fragment abstracts another proton of the CH_2=CH fragment to form a CH≡$CH^-\cdots H_2O$ intermediate complex, the final products will be electron, CH≡CH, and H_2O because of the unstable CH≡CH^- [4]. Briefly, the major reaction process leading to the H_2^+ abstraction channel can be summarized as follow, $O^- + C_2H_4$ (reactants) → $[O\cdots H\cdots CH{=}CH_2]^-$ (TS1) → $OH^-\cdots$CH=CH_2 (dynamic IM3) → CH_2=$C^-\cdots H_2O$ (product-like

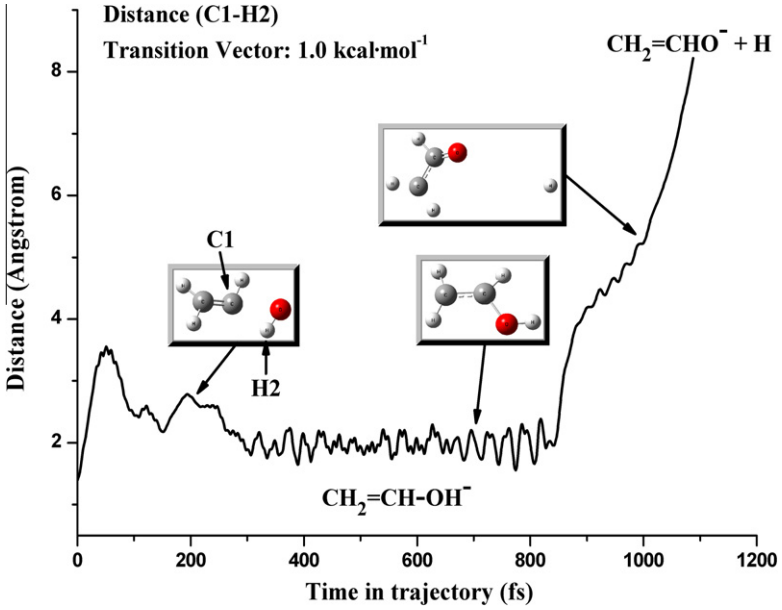

Fig. 2. Distances between C1 atom and H2 atom along a typical trajectory which corresponds to the CH_2=CHO^- + H channel. The trajectory involves a dynamic intermediate complex of CH_2=CH—OH^- like IM2 in Fig. 1. Molecular structures of three points along this trajectory are also depicted.

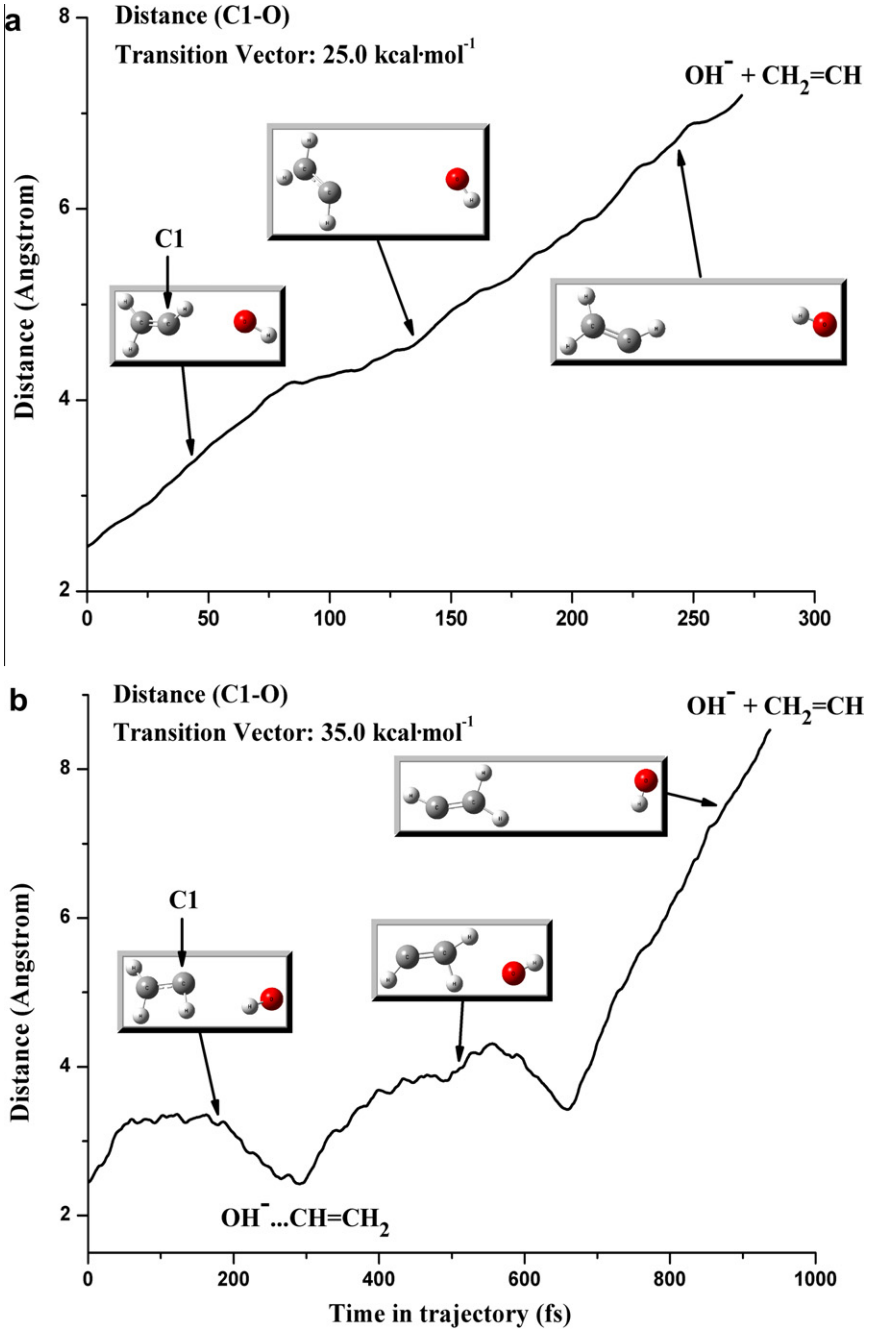

Fig. 3. Distances between C1 atom and O atom along two typical trajectories, both of which lead to the $OH^- + CH_2{=}CH$ as products. The first one shows a direct reaction process without involving any intermediate complex (a), and the second one corresponds to a reaction process involving the dynamic intermediate complex of $OH^-\cdots CH{=}CH_2$ (b). Molecular geometries of six points along these two trajectories are also shown.

dynamic IM4) → $CH_2{=}C^- + H_2O$ (products). The key mechanism from the dynamic IM3 to the product-like dynamic IM4 can be viewed as the "roaming" OH^- fragment abstracts a proton of the $CH_2{=}CH$ fragment, which has been highlighted in previous theoretical works [36,37]. Therefore, the "roaming" OH^- fragment provides a reasonable explanation for the H_2^+ abstraction channel, which is consistent with the potential energy profiles [1,14].

3.4. Driven energies for the dynamic reaction pathways

When the relatively low energies, e.g. 1.0 and 5.0 kcal mol^{-1}, added on the transition vector of the TS1, the title reaction prefers to follow the MEP approximately as the IRC calculation suggests. As a result, the reactive trajectory will be trapped in the deep $CH_2{=}CH{-}OH^-$ potential well for a period of time, and the major products of $CH_2{=}CHO^- + H$ will be formed subsequently via the cleavage of the O—H bond. On the contrary, if the energy added on the transition vector is relatively high, e.g. 25.0 and 35.0 kcal mol^{-1}, it tends to drive the trajectory bypassing the deep $CH_2{=}CH{-}OH^-$ potential well to form the products of $OH^- + CH_2{=}CH$. However, on the exit-channel PES, the strong ion–dipole interaction energy between the OH^- and $CH_2{=}CH$ fragments will attract the dissociating OH^- fragment roaming back. Subsequently, the roaming OH^- fragment abstracts a proton of the $CH_2{=}CH$ fragment to form the $CH_2{=}C^-\cdots H_2O$ intermediate complex, which decomposes to the $CH_2{=}C^-$ and H_2O finally.

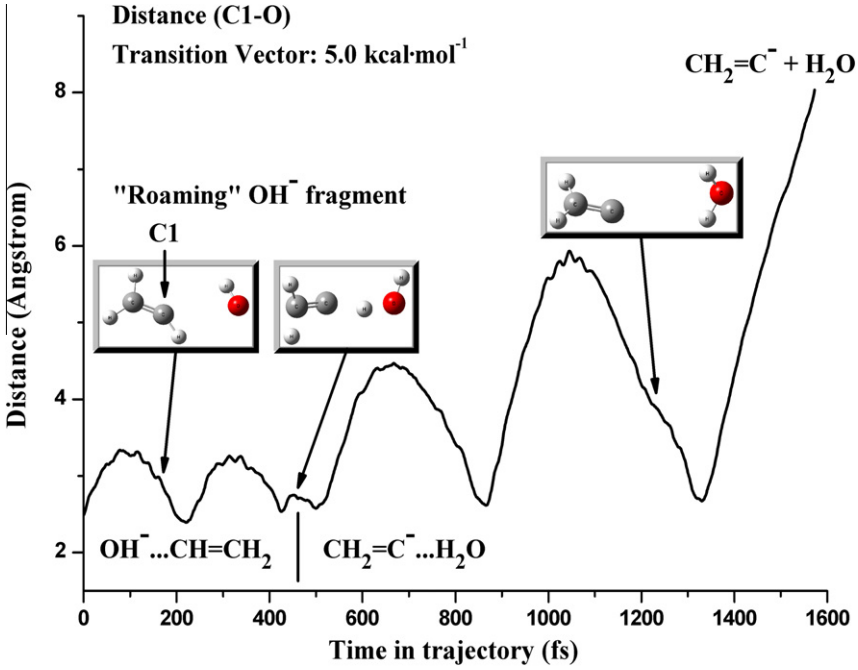

Fig. 4. Distances between C1 atom and O atom along a typical trajectory which leads to $CH_2{=}C^- + H_2O$ as products. The key reaction process is that the "roaming" OH^- fragment abstracts a proton of the $CH_2{=}CH$ fragment to form the dynamic intermediate complex of $CH_2{=}C^-\cdots H_2O$. Three molecular structures are also exhibited along this trajectory.

3.5. Comments on the present BOMD simulations

In our previous theoretical investigations on the title reaction [14], we have optimized the stationary points on the PES at the B3LYP/6-31+G(d,p) and B3LYP/aug-cc-pVTZ levels of theory, respectively. Based on the molecular structures obtained at the B3LYP/6-31+G(d,p) level, we have mapped the potential energy profile using the G3MP2B3 method. Unfortunately, the G3MP2B3 method cannot be applied to the BOMD simulation, while the B3LYP/aug-cc-pVTZ level of theory is too time-consuming to be employed in trajectory calculation. Therefore, the level of theory we utilized here is the B3LYP/6-31+G(d,p), which can balance the computational accuracy with cost. At each step along the trajectory, the wave function of the reactive system is converged to the ground state and no multi-configuration wave function is taken into account. Moreover, as mentioned above, the BOMD simulations based on the general *ab initio* and density functional theory (DFT) methods are incapable of modeling the associative electron detachment process.

In general, a global analytical PES for a reactive system is expected to make the trajectory calculation much easier. However, it is impossible to construct the global analytical PES for O^- with $CH_2{=}CH_2$ because of many degrees of freedom. Therefore, we choose the BOMD method to avoid the construction of the global analytical PES. To model a reaction between anion and molecule, especially for the open-shell reactive system, the SCF convergence problem is an ordinary issue in the technical view, especially for the regions near to the dissociation limits. We have only calculated a total of 220 trajectories in the present work due to the computational cost and SCF convergence problems encountered in the Gaussian 03 program [24]. A total of 19 trajectories have been discarded due to the SCF convergence errors (Appendix A. Supplementary material). We cannot obtain accurate branching ratio for each production channel and energy distributions for the corresponding products based on the present 220 trajectories. Nevertheless, we can deduce the dominant production channels and the corresponding reaction mechanisms from the dynamic reaction pathways. Most importantly, these dynamic reaction pathways are able to provide deeper insights into the reaction mechanism rather than the previous potential energy profile at the G3MP2B3 level [14].

4. Conclusions

The dynamic reaction pathways and the corresponding reaction mechanisms after passing the $[O\cdots H\cdots CH{=}CH_2]^-$ barrier (TS1) for the reaction of O^- with $CH_2{=}CH_2$ have been studied with the BOMD simulations. As illuminated in our calculations, the dominant products are confirmed to be $CH_2{=}CHO^-$ and H when the energy added on the transition vector of the TS1 is 1.0 kcal mol^{-1}. With the energy added on the transition vector increased to 5.0 kcal mol^{-1}, the $CH_2{=}C^- + H_2O$ production channel becomes more important. The major production channels are $OH^- + CH_2{=}CH$ and $CH_2{=}C^- + H_2O$ when the energies added on the transition vector are both 25.0 and 35.0 kcal mol^{-1}.

These reaction processes mentioned above should pass through the IM2 according to the static reaction pathway revealed by the IRC profile. However, our BOMD simulations show that some reaction processes undergo the different dynamic reaction pathways. For the $OH^- + CH_2{=}CH$ production channel, the relatively high energy added on the transition vector of the TS1 makes the dynamic reaction pathways depart from the MEP and bypass the deep $CH_2{=}CH{-}OH^-$ potential well. This dynamic reaction mechanism is very important for the H-atom abstraction channel, because it provides insight into the direct H-atom abstraction process between O^- and organic molecule. In addition, the "roaming" OH^- fragment provides a reasonable explanation for the H_2O production channels. In summary, the current BOMD simulations reveal more comprehensive reaction mechanisms for the title reaction than the IRC calculation.

Acknowledgements

The financial supports from the National Natural Science Foundation of China (NSFC, Nos. 20603033, 10979042) and National

Key Basic Research Special Foundation (NKBRSF, No. 2007C B815204) are gratefully acknowledged. The authors also acknowledge the supercomputing center of University of Science and Technology of China (USTC) for providing the computational resources.

Appendix A. Supplementary data

Supplementary data associated with this article can be found, in the online version, at doi:10.1016/j.theochem.2010.07.023.

References

[1] J. Lee, J.J. Grabowski, Chem. Rev. 92 (1992) 1611. and references therein.
[2] M. Born, S. Ingemann, N.M.M. Nibbering, Mass Spectrom. Rev. 16 (1997) 181.
[3] Y. Guo, J.J. Grabowski, Int. J. Mass Spectrom. Ion Processes 97 (1990) 253.
[4] M.J. Jensen, U.V. Pedersen, L.H. Andersen, Phys. Rev. Lett. 84 (2000) 1128.
[5] M. Born, S. Ingemann, N.M.M. Nibbering, J. Am. Chem. Soc. 116 (1994) 7210.
[6] D.K. Bohme, L.B. Young, J. Am. Chem. Soc. 92 (1970) 3301.
[7] J.A.D. Stockdale, R.N. Compton, P.W. Reinhardt, Int. J. Mass Spectrom. Ion Phys. 4 (1970) 401.
[8] J.H. Futrell, T.O. Tiernan, in: J.L. Franklin (Ed.), Ion-Molecule Reactions, vol. 2, Butterworths, London, 1972 (Chapter 11).
[9] D.A. Parkes, J. Chem. Soc. Faraday Trans. I 68 (1972) 613.
[10] G.C. Goode, K.R. Jennings, Adv. Mass Spectrom. 6 (1974) 797.
[11] W. Lindinger, D.L. Albritton, F.C. Fehsenfeld, E.E. Ferguson, J. Chem. Phys. 63 (1975) 3238.
[12] J.H.J. Dawson, K.R. Jennings, J. Chem. Soc. Faraday Trans. II 72 (1976) 700.
[13] A.A. Viggiano, J.F. Paulson, J. Chem. Phys. 79 (1983) 2241.
[14] F. Yu, Y. Zhao, Y. Wang, X. Zhou, S. Liu, Acta Chim. Sin. 65 (2007) 899.
[15] X. Wang, F. Yu, D. Xie, S. Liu, X. Zhou, Acta Chim. Sin. 66 (2008) 2499.
[16] Y. Zhao, Y. Zhang, Y. Chen, J. Mol. Struct. (THEOCHEM) 867 (2008) 28.
[17] L. Sun, K. Song, W.L. Hase, Science 296 (2002) 875.
[18] J.G. López, G. Vayner, U. Lourderaj, S.V. Addepalli, S. Kato, W.A. de Jong, T.L. Windus, W.L. Hase, J. Am. Chem. Soc. 129 (2007) 9976.
[19] U. Lourderaj, K. Park, W.L. Hase, Int. Rev. Phys. Chem. 27 (2008) 361.
[20] U. Lourderaj, W.L. Hase, J. Phys. Chem. A 113 (2009) 2236.
[21] K. Bolton, W.L. Hase, G.H. Peslherbe, in: D.L. Thompson (Ed.), Modern Methods for Multidimensional Dynamics Computations in Chemistry, World Scientific, Singapore, 1998, pp. 143–189.
[22] H.B. Schlegel, J. Comput. Chem. 24 (2003) 1514.
[23] H.B. Schlegel, Bull. Korean Chem. Soc. 24 (2003) 837.
[24] M.J. Frisch, G.W. Trucks, H.B. Schlegel, G.E. Scuseria, M.A. Robb, J.R. Cheeseman, J.A. Montgomery Jr., T. Vreven, K.N. Kudin, J.C. Burant, J.M. Millam, S.S. Iyengar, J. Tomasi, V. Barone, B. Mennucci, M. Cossi, G. Scalmani, N. Rega, G.A. Petersson, H. Nakatsuji, M. Hada, M. Ehara, K. Toyota, R. Fukuda, J. Hasegawa, M. Ishida, T. Nakajima, Y. Honda, O. Kitao, H. Nakai, M. Klene, X. Li, J.E. Knox, H.P. Hratchian, J.B. Cross, V. Bakken, C. Adamo, J. Jaramillo, R. Gomperts, R.E. Stratmann, O. Yazyev, A.J. Austin, R. Cammi, C. Pomelli, J.W. Ochterski, P.Y. Ayala, K. Morokuma, G.A. Voth, P. Salvador, J.J. Dannenberg, V.G. Zakrzewski, S. Dapprich, A.D. Daniels, M.C. Strain, O. Farkas, D.K. Malick, A.D. Rabuck, K. Raghavachari, J.B. Foresman, J.V. Ortiz, Q. Cui, A.G. Baboul, S. Clifford, J. Cioslowski, B.B. Stefanov, G. Liu, A. Liashenko, P. Piskorz, I. Komaromi, R.L. Martin, D.J. Fox, T. Keith, M.A. Al-Laham, C.Y. Peng, A. Nanayakkara, M. Challacombe, P.M.W. Gill, B. Johnson, W. Chen, M.W. Wong, C. Gonzalez, J.A. Pople, Gaussian 03, Revision C.02, D.01, and D.02, Gaussian, Inc., Wallingford, CT, 2004.
[25] G.B. Bacskay, Chem. Phys. 61 (1981) 385.
[26] C. Lee, W. Yang, R.G. Parr, Phys. Rev. B 37 (1988) 785.
[27] A.D. Becke, J. Chem. Phys. 98 (1993) 5648.
[28] M. Yamamoto, K. Yamashita, M. Sadakata, J. Mol. Struct. (THEOCHEM) 634 (2003) 31.
[29] F. Yu, L. Wu, S. Liu, X. Zhou, J. Mol. Struct. (THEOCHEM) 947 (2010) 1.
[30] J.M. Millam, V. Bakken, W. Chen, W.L. Hase, H.B. Schlegel, J. Chem. Phys. 111 (1999) 3800.
[31] V. Bakken, J.M. Millam, H.B. Schlegel, J. Chem. Phys. 111 (1999) 8773.
[32] W.L. Hase, in: P.v.R. Schleyer, N.L. Allinger, T. Clark, J. Gasteiger, P.A. Kollman, H.F. Scheafer III, P.R. Schreiner (Eds.), Encyclopedia of Computational Chemistry, Wiley, Chichester, UK, 1998, pp. 402–407.
[33] G.H. Peslherbe, H. Wang, W.L. Hase, Adv. Chem. Phys. 105 (1999) 171.
[34] S.C. Ammal, H. Yamataka, M. Aida, M. Dupuis, Science 299 (2003) 1555.
[35] R.S. Mulliken, J. Chem. Phys. 23 (1955) 1833.
[36] A. Fernández-Ramos, J.A. Miller, S.J. Klippenstein, D.G. Truhlar, Chem. Rev. 106 (2006) 4518.
[37] L.B. Harding, Y. Georgievskii, S.J. Klippenstein, J. Phys. Chem. A 114 (2010) 765.